Engineering Structures 297 (2023) 116975

Contents lists available at ScienceDirect

Engineering Structures

journal homepage: www.elsevier.com/locate/engstruct

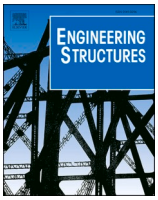

A comprehensive evaluation of the effects of bamboo nodes on the mechanical properties of bamboo culms

Xinmiao Meng [a,*], Zhancheng Zhang [a], Youde Wu [b], Feiyang Xu [c], Peng Feng [b,*]

[a] Department of Civil Engineering, Beijing Forestry University, Beijing 100083, China
[b] Department of Civil Engineering, Tsinghua University, Beijing 100084, China
[c] College of Materials Science and Technology, Beijing Forestry University, Beijing 100083, China

ARTICLE INFO

Keywords:
Bamboo node
Diaphragm
Fiber morphology
Mechanical property
Failure modes

ABSTRACT

Architectural pavilions made of round bamboo are undergoing rapid development due to their appealing appearance and low carbon footprint, but their structural analysis is challenging due to the existence of bamboo nodes. Generally, bamboo nodes provide positive effects on the mechanical behavior of bamboo culms in terms of evolution. However, the loading conditions of bamboo culms used in buildings greatly differ from the natural conditions. Some studies have been conducted on this issue but come to different conclusions. In this regard, this work conducts a comprehensive study on the effects of bamboo nodes on the mechanical properties of bamboo culms. A total of 168 specimens divided into four types were tested, including compressive, tensile and shear tests parallel to the grain and radial compressive tests. The load–displacement curves and failure modes were analyzed. The analysis of variance method was used to evaluate the effects of bamboo nodes on the mechanical properties. A comprehensive discussion based on fiber morphology is presented to explain the effects of nodes under different load conditions. Additionally, the fiber distribution in the diaphragm was observed, and the compressive strength of the diaphragm was tested. It was found that the bamboo node had significant effects on the tensile strength and radial compressive modulus. Compared to the bamboo culm without nodes, the tensile strength of bamboo culm with nodes decreased by 47%, while the node could improve the pipe stiffness by 123%. In compressive and shear tests parallel to the grain, the bamboo node showed slight effects on the strength. The differences in both strengths were all within 9% in value. Based on the geometric model, the relationship between the fiber morphology and the mechanical properties was built. In short, the bamboo node showed less improvement in compressive and shear tests parallel to the grain but should be carefully considered in tensile conditions due to its weakening effect.

1. Introduction

Bamboo is a promising building material in terms of its carbon sequestration characteristics to reduce global greenhouse gas emissions [1]. In particular, round bamboo shows a lower carbon footprint than engineered bamboo due to its simple procedure and lower energy consumption in the manufacturing process. In addition, round bamboo has been widely used to construct curvilinear pavilions due to its thermal-bending property [2]. In this regard, lots of round bamboo pavilions have been constructed in China. However, it is always a challenge to conduct structural analysis of round bamboo structures due to the existence of bamboo nodes. The bamboo node is complex in geometric structures [3,4], as shown in Fig. 1. In the natural environment, the raw bamboo culm is similar to a cantilever beam, and defection is often caused by self-weight and wind load [5]. Bamboo nodes are vital for the strength and stability of bamboo culms [6–9]. Nonetheless, the loading conditions of bamboo culms in full-culm bamboo structures differ greatly from natural conditions [6–14].

In this regard, the effects of bamboo nodes under different loading conditions should be reconsidered. As shown in Table 1, some researchers have noted the effects of bamboo nodes on the strength of bamboo culms, but the conclusions were inconsistent and disputed. It was reported that the existence of bamboo nodes had a positive [6,13] or negative [15,16] effect on the compressive strength, but the effects of the strength in most cases [6,13,15] were not obvious. For tensile strength parallel to the grain, most of the studies [6,13,15,17] showed

* Corresponding authors.
E-mail addresses: mengxinmiao@bjfu.edu.cn (X. Meng), fengpeng@tsinghua.edu.cn (P. Feng).

https://doi.org/10.1016/j.engstruct.2023.116975

Available online 3 October 2023
0141-0296/© 2023 Elsevier Ltd. All rights reserved.

that the tensile strength of the coupons with nodes was lower than that of the internode. However, Chen and Luo [18] reported that the node was stronger than the internode due to the coarser fiber bundles, higher fiction of fibers, and hierarchical fibrous woven structure at the node. For the shear strength parallel to the grain, some researchers [6,15] believed that the bamboo node could strengthen the longitudinal shear strength of specimens, while other researchers [13,16,17] considered that the bamboo node slightly weakened the shear strength parallel to the grain.

Most studies have focused on the effects of nodes on compressive, tensile and shear strengths parallel to the grain, but the radial compressive performance of bamboo culm is also important in engineering applications [19–22]. In a full-culm bamboo structure, the bamboo culms mainly bear radial loads at the cross-lap joints. Nevertheless, few studies have been conducted to evaluate the effects of nodes on the radial properties of bamboo [23]. Therefore, it is necessary to carry out radial compressive tests to determine the effects of nodes and thus provide a reference for the layout arrangement of bamboo culms in cross-lap joints.

In this paper, a total of 168 specimens were tested in four types to evaluate the effects of nodes on the mechanical properties of natural bamboo culms, including compressive, tensile and shear tests parallel to the grain and radial compressive tests. The load–displacement curves and the failure modes were analyzed. In addition, the compressive strength of the bamboo diaphragm was obtained by a compressive test. Finally, a comprehensive discussion based on fiber morphology was presented to explain the mechanical behavior of compressive, tensile and shear specimens with nodes.

2. Experimental programs

2.1. Materials

In this work, four-year-old Moso bamboo (*Phyllostachys edulis*) culms were obtained from Hubei Province, China. Both ends of the raw bamboo were cut off in a length of 1.0 m to avoid the impact of shape distortion. The remaining culm was evenly longitudinally divided into three parts, denoted as B (bottom), M (middle), and T (top). The wall thickness ranged from 6 mm to 9 mm, and the diameter of the bamboo culm ranged from 60 mm to 80 mm. All specimens were placed in ambient conditions for more than one week before the tests to reduce the difference in moisture content. The moisture content was between 10.5% and 15.2%, as measured according to ISO 22157–2019 [24]. All specimens in each test were taken from the same bamboo culm to reduce the influence of material variation on the test results.

2.2. Design and preparation of specimens

Table 2 shows that a total of 168 specimens were prepared for four different mechanical tests. Each type of test included specimens that were selected evenly from the top, middle, and bottom of the bamboo. Specifically, for a test with six specimens, two were selected from the top, two from the middle, and two from the bottom of the bamboo. The compressive specimens were obtained from four bamboo culms designated A, B, C, and D, as shown in Fig. 2(a), where bamboo culms A and B were prepared for the specimens of 100 mm height, and bamboo culms C and D were allocated for the specimens of 200 mm height. The tensile specimens were obtained from two bamboo culms designated E and F, as shown in Fig. 2(b). The shear specimens were obtained from two bamboo culms designated G and I, in which the diaphragms of bamboo I were removed, as shown in Fig. 2(c). The radial compressive specimens were obtained from two bamboo culms designated H and J, in which the diaphragms of bamboo J were also removed.

Table 1
Effects of nodes on the mechanical properties of bamboo culms.

Reference	Compressive strength parallel to the grain Effect		Tensile strength parallel to the grain Effect		Shear strength parallel to the grain Effect	
Shao et al. [6]	Positive	6%	Negative	–33%	Positive	3%
Oka et al. [15]	Positive	4%	Negative	−57%	Negative	−2%
Sivero and Jakranod [17]	–	–	Negative	−54%	Negative	−5%
Huang et al. [16]	Negative	−36%	–	–	Negative	−50%
Chen and Luo [18]	–	–	Positive	23%	–	–
Liu et al. [13]	Positive	5%	Negative	−14%	Positive	2%

2.3. Experimental setup and instrumentation

The experimental setup is shown in Fig. 2. Compressive and tensile tests parallel to the grain were carried out through a 300 kN universal testing machine, while shear tests parallel to the grain and radial compressive tests were carried out using a 100 kN testing machine. For compressive tests, a spherical hinge was used to reduce the influence of the misalignment of the specimens, and the intermediate layer was applied between the steel plate and the specimen end to minimize the radial friction restraint of the steel plate according to ISO 22157–2019, as shown in Fig. 2(a). The compressive tests were performed with a loading rate of 6 mm/min. The tensile tests parallel to the grain were carried out in accordance with JGT 199–2007 [25] with a loading rate of 6 mm/min, as shown in Fig. 2(b). The shear tests parallel to the grain were carried out in accordance with ISO 22157–2019 with a loading rate of 0.6 mm/min. To ensure accurate testing, it is essential that the specimen is positioned with its axis in alignment with the loading axis of the machine and that the center of the specimen coincides with that of the shear plates. Prior to testing, a minimal load of no more than 1 % of the expected failure load should be applied to seat the specimen. For the radial compressive tests, the loading was carried out along the minor

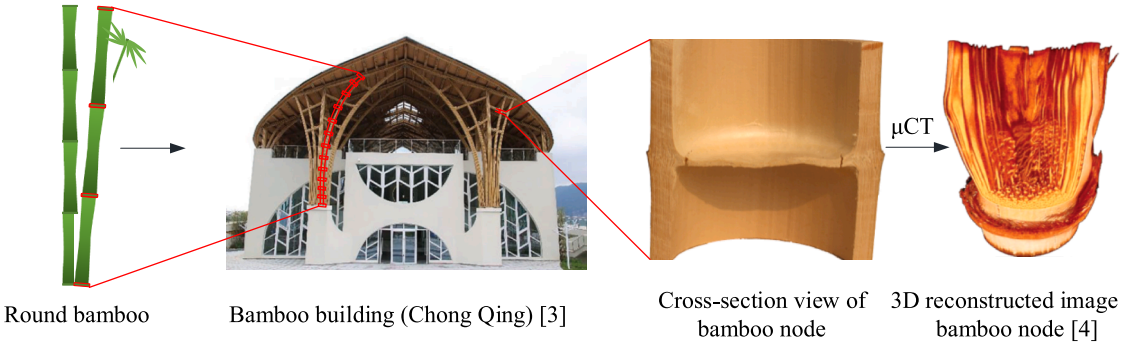

Fig. 1. Multi-scale structures of the bamboo node.

Table 2
Details of the specimens.

Specimen group	Culm No.	Node	Test standard	Loading rate (mm/min)	Strength calculation	Specimen number
Compressive test parallel to the grain	Bamboo A	Node	ISO 22157–2019	6	$f_c = \frac{F_{ult}}{A}$	6
		Internode				6
	Bamboo B	Node				6
		Internode				6
	Bamboo C	Node				6
		Internode				6
	Bamboo D	Node				6
		Internode				6
Tensile test parallel to the grain	Bamboo E	Node	JGT 199–2007	6	$f_t = \frac{F_{ult}}{bt}$	6
		Internode				6
	Bamboo F	Node				6
		Internode				6
Shear test parallel to the grain	Bamboo G	Node	ISO 22157–2019	0.6	$f_v = \frac{F_{ult}}{\sum(\delta \times L)}$	12
		Internode				12
	Bamboo I	Without diaphragm				12
		Internode				12
Radial compressive test	Bamboo H	Node	ASTM D2412-96a	2	$PS = \frac{F}{\Delta y}$	12
		Internode				12
	Bamboo J	Without diaphragm				12
		Internode				12

Note: f_c is the compression strength parallel to the fibers, F_{ult} is the maximum load at which the specimen fails, A is the cross-sectional area of the culm, f_t is the tension strength parallel to the direction of the fibers, b is the width of the tension test specimen gauge region, t is the thickness of the tension test specimen gauge region, f_v is the shear strength parallel to the fibers, $\sum(\delta \times L)$ is the sum of the four measured areas at the shear planes, PS is the pipe stiffness, F is the load applied to the pipe to produce a given percentage deflection, Δy is the measured change in the inside diameter in the direction of the load.

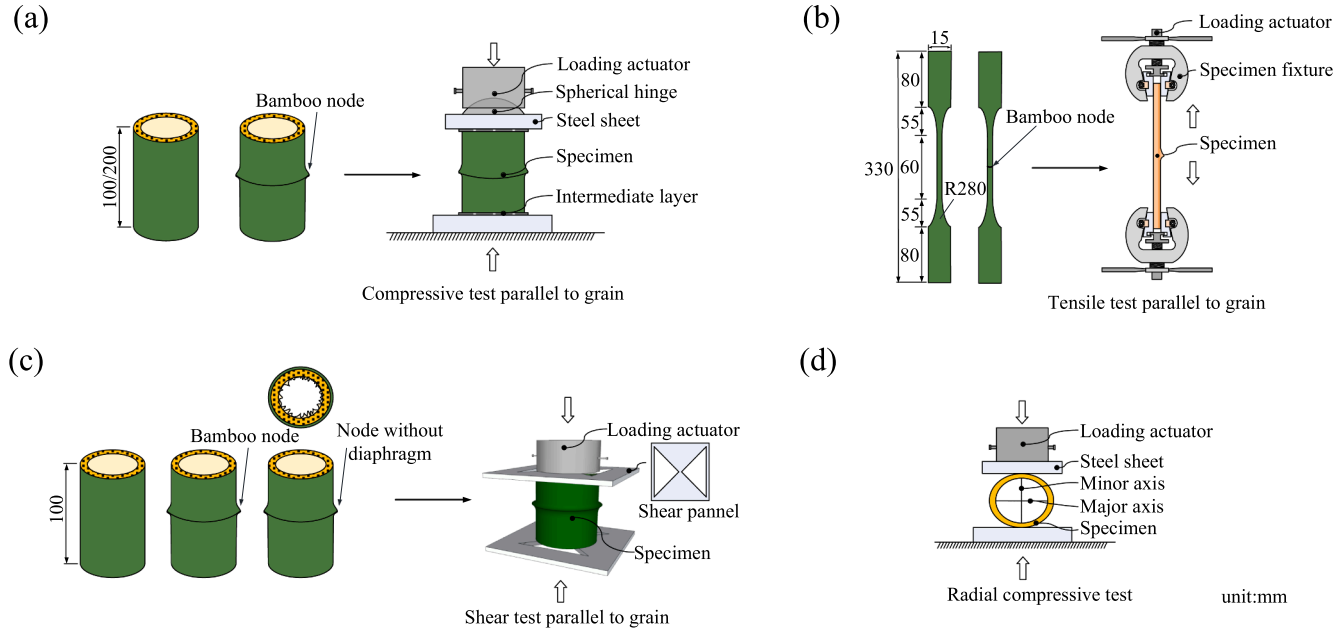

Fig. 2. Experimental setup and instrumentation: (a) compressive test, (b) tensile test, (c) shear test parallel to the grain, and (d) radial compressive test.

axis direction in terms of the elliptical cross section of the specimens. The loading rate in the radial compressive tests was set as 2 mm/min following GB/T 9647–2015 [26]. The pipe stiffness in radial compressive tests was calculated in accordance with ASTM D2412-96a [27].

Strain gauges were placed on the inner and outer surfaces of radial compressive specimens to measure the strain values in critical regions. The layout of the strain gauges is shown in Fig. 3. The displacement was recorded by the displacement transducers installed at the loading actuator.

3. Experimental results

3.1. Experimental observation and failure modes

In compressive specimens parallel to the grain, the specimens of 100 mm height were observed to fail in both global and local buckling modes, as shown in Fig. 4(a) and (b). Due to the Poisson effect and splitting throughout the entire height, the internode specimens exhibited buckling at the middle of the height. The buckling mode resembled the elephant-foot buckling seen in thin metal cylindrical shell structures. Fully developed longitudinal splitting was the primary cause of specimen failure. Fig. 4(b) displays the typical failure mode of the node specimens with a height of 100 mm. Owing to the circumferential restraint of the bamboo node, splitting and local buckling initially

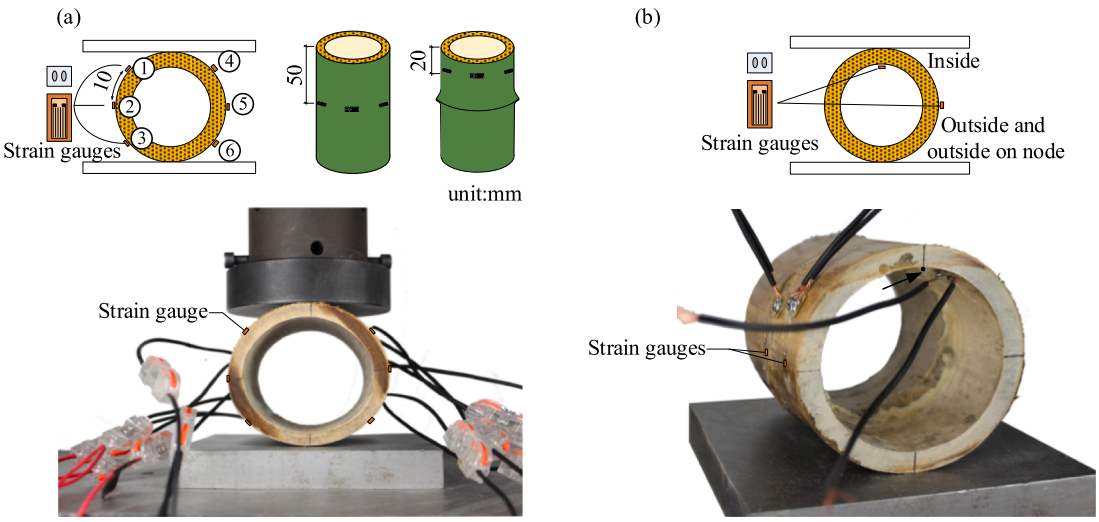

Fig. 3. The layout of strain gauges on: (a) bamboo H, and (b) bamboo J.

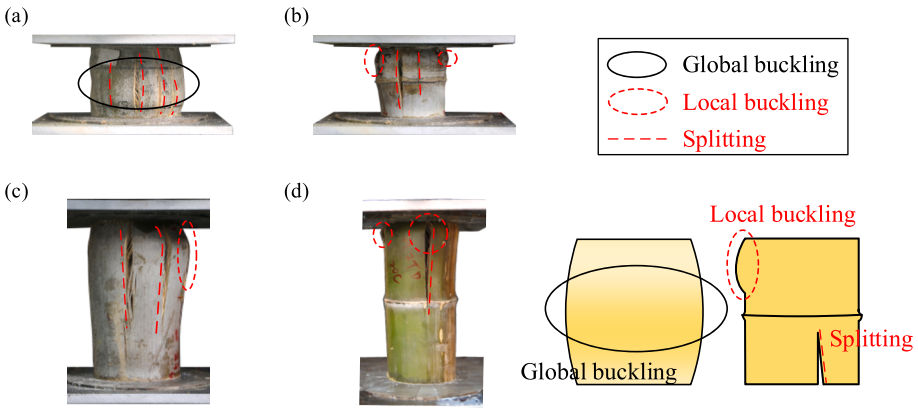

Fig. 4. Typical failure modes of compressive specimens: (a) 100 mm height internode specimen, (b) 100 mm height node specimen, (c) 200 mm height internode specimen, and (d) 200 mm height node specimen.

occurred at the specimen ends. As the axial displacement increased to its maximum value, the specimens underwent longitudinal splitting across the node, leading to failure. The specimens with a height of 200 mm failed through splitting accompanied by local buckling, as shown in Fig. 4(c) and (d). For internode specimens, splitting and local buckling occurred first at one end of the specimen, followed by the development of longitudinal splitting and lateral displacement. Once the splitting had developed through approximately half the specimen height, failure occurred. For the node specimens, splitting and buckling occurred at one or both ends of the specimen, and failure was caused by the development of splitting and buckling across the node region.

Fig. 5(a) shows the typical failure mode of internode specimens in tensile tests. When the axial displacement increased to the maximum value, the fibers at the inside of the bamboo culm first fractured, and a small transversal crack occurred, followed by the development of longitudinal cracks until failure. For the node specimens, two failure modes were observed, as shown in Fig. 5(b). In failure mode I, the transverse crack first occurred near the node, and then the crack began to develop longitudinally until failure, and this was similar to the tensile internode specimen. In failure mode II, the initial crack appeared at the node and was quickly followed by the rupture of the whole node with a rough failure surface.

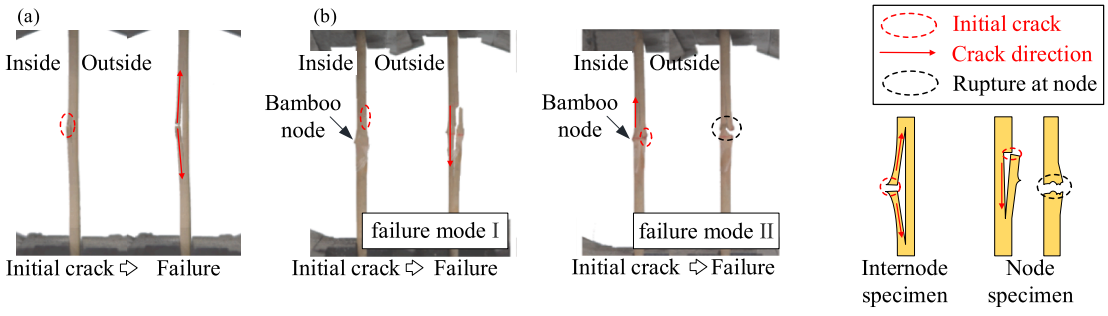

Fig. 5. Typical failure modes of tensile specimens: (a) tensile internode specimen, and (b) failure mode I and II of tensile node specimen.

The failure modes of shear specimens parallel to the grain are shown in Fig. 6. A series of parallel lines were drawn perpendicular to the intended shear surface to assist the observation of the relative slip. All the shear specimens experienced sudden shear failure in one of the four shear surfaces. Fig. 6(a) shows the failure mode of internode specimens. The parallel lines were obviously dislocated, indicating a large relative slip at the shear surface. For the node specimens with or without the diaphragm, no obvious dislocation of the parallel line appeared until the peak load. When reaching the peak load, a shear crack suddenly occurred at the shear surface with a loud sound, as shown in Fig. 6(b) and (c).

The failure modes of the radial compressive specimens are shown in Fig. 7. For the internode specimens, one or two splitting cracks occurred at the outer surface during the loading process, and the cracks were close to the major axis, as shown in Fig. 7(a). The specimen failed when one of the splits developed through the bamboo culm. Fig. 7(b) shows the failure mode of the node specimens. The distribution of splitting cracks was similar to that of the internode specimens. When reaching the peak load, a crack suddenly developed through the diaphragm along the minor axis. Fig. 7(c) shows the failure mode of the node specimens without the diaphragm. During the loading process, splitting inside the bamboo wall first occurred at or near the minor axis. Then, splitting outside the bamboo wall occurred. The distribution of splitting cracks was more complex.

3.2. Load-displacement relationships

The load–displacement curves were demonstrated for compressive, tensile and shear tests parallel to the grain, as shown in Fig. 8. The typical curves were selected from the tested specimens, based on their similarity to the average normalized curve. These selected curves were characterized by their smooth profiles and representative trends. The selected typical curve should exhibit a linear region within the displacement range, as well as strain hardening or brittle fracture when the material reaches its maximum strength.

Fig. 8(a) shows the typical load–displacement curves of compressive specimens. The internode and node specimens exhibited similar load–displacement relationships. The initial nonlinear stage occurred in some specimens due to fabrication error and material densification. After that, the curves entered the linear stage. When the load reached 90% of the maximum load, the stiffness first decreased rapidly and then gradually until reaching the peak point. After the peak point, the curve entered the descending stage. In this stage, the curves of the 100 mm internode specimens first decreased slowly with the development of splitting and buckling. When the splitting cracks developed through the full height, the curve began to decrease rapidly until the specimen failed. However, for 100 mm node specimens, the curves began to decrease rapidly once the splitting developed across the bamboo node. In addition, for 200 mm internode specimens, when the splitting cracks developed through half of the height of the specimen, the curves began to rapidly decrease, while the curve rapidly descended when the splitting crossed the node for 200 mm node specimens.

Fig. 8(b) shows the load–displacement curves of the tensile specimens. For both internode and node specimens, the curves linearly developed with increasing load. When reaching the tensile strength, the specimens failed with a sharp drop in the load due to the brittle fracture of the fibers.

Fig. 8(c) shows the load–displacement curves of the shear specimens. The curves were composed of four stages, including the initial stage, linear stage, softening stage and sharp-drop stage. After the nonlinear initial stage due to the fabrication gaps and material densification, the curves linearly developed. When approaching the failure load, the slope gradually decreased with rapid development of relative slip at shear surfaces. Then, the curves showed a sharp drop due to the sudden failure of the shear surface.

Fig. 8(d) shows the load–displacement curves of the radial compressive specimens. For internode specimens, the curves showed linear development at first. When a splitting crack occurred on the surface, the curve showed a drop off, but the load increased again after that. After the development of a crack through the bamboo culm wall, the specimen lost its bearing capacity, resulting in a sharp drop in the curve. For node specimens with a diaphragm, the curves were also linear at the beginning, but the slope was greater than that of internode specimens. When approaching the peak load, the curves had a slight drop off with splitting appearing at the outside of the bamboo wall. Then, the load increased again to the peak point. After that, the curves had a sharp drop due to the sudden fracture of the diaphragm along the minor axis. For node specimens without a diaphragm, the curves were similar to those of internode specimens, but the peak load was reached when the first splitting occurred.

Table 3 lists the average strength and increment of the bamboo specimens. In terms of compressive strength, there was hardly any difference between the internode and node specimens with heights of 100 or 200 mm. The average strength difference was less than 5%. In contrast, the internode specimens exhibited significantly greater tensile strength than the node specimens, as these were decreased by 43–50%. The shear strength of the bamboo node slightly increased, regardless of whether the diaphragm was removed, with strength changes within a 9% range. For radial compressive specimens in bamboo H, the existence of the diaphragm led to a significant improvement in pipe stiffness by the bamboo node, with the pipe stiffness of node specimens being 123% higher than that of the internode specimens. However, for bamboo J, the removal of the diaphragm weakened the improved effect of the bamboo node on the pipe stiffness, with the pipe stiffness of the node specimens being only approximately 6% higher than that of the internode specimens.

4. Analysis

4.1. Strength and pipe stiffness

The boxplots of the strength and pipe stiffness of the specimens are shown in Fig. 9. The compressive strength of the node and internode specimens is shown in Fig. 9(a). The average compressive strength of specimens of 200 mm height was approximately 18% (internode) and 14% (node) lower than that of 100 mm specimens mainly due to the higher slenderness ratio. However, the average compressive strength of internode specimens was close to that of node specimens at the same

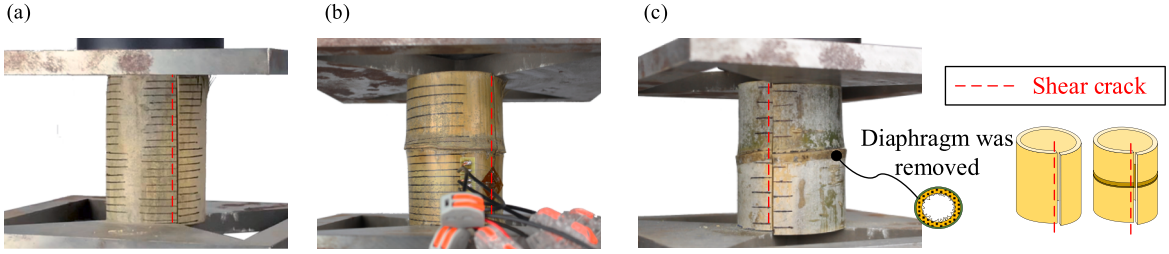

Fig. 6. Typical failure modes of shear specimens: (a) internode specimen, (b) node specimen with diaphragm, and (c) node specimen without diaphragm.

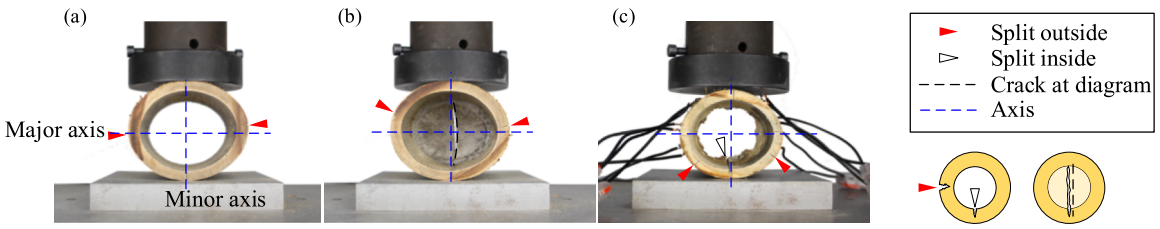

Fig. 7. Typical failure modes of radial compressive specimens: (a) internode specimen, (b) node specimen with diaphragm, and (c) node specimen without diaphragm.

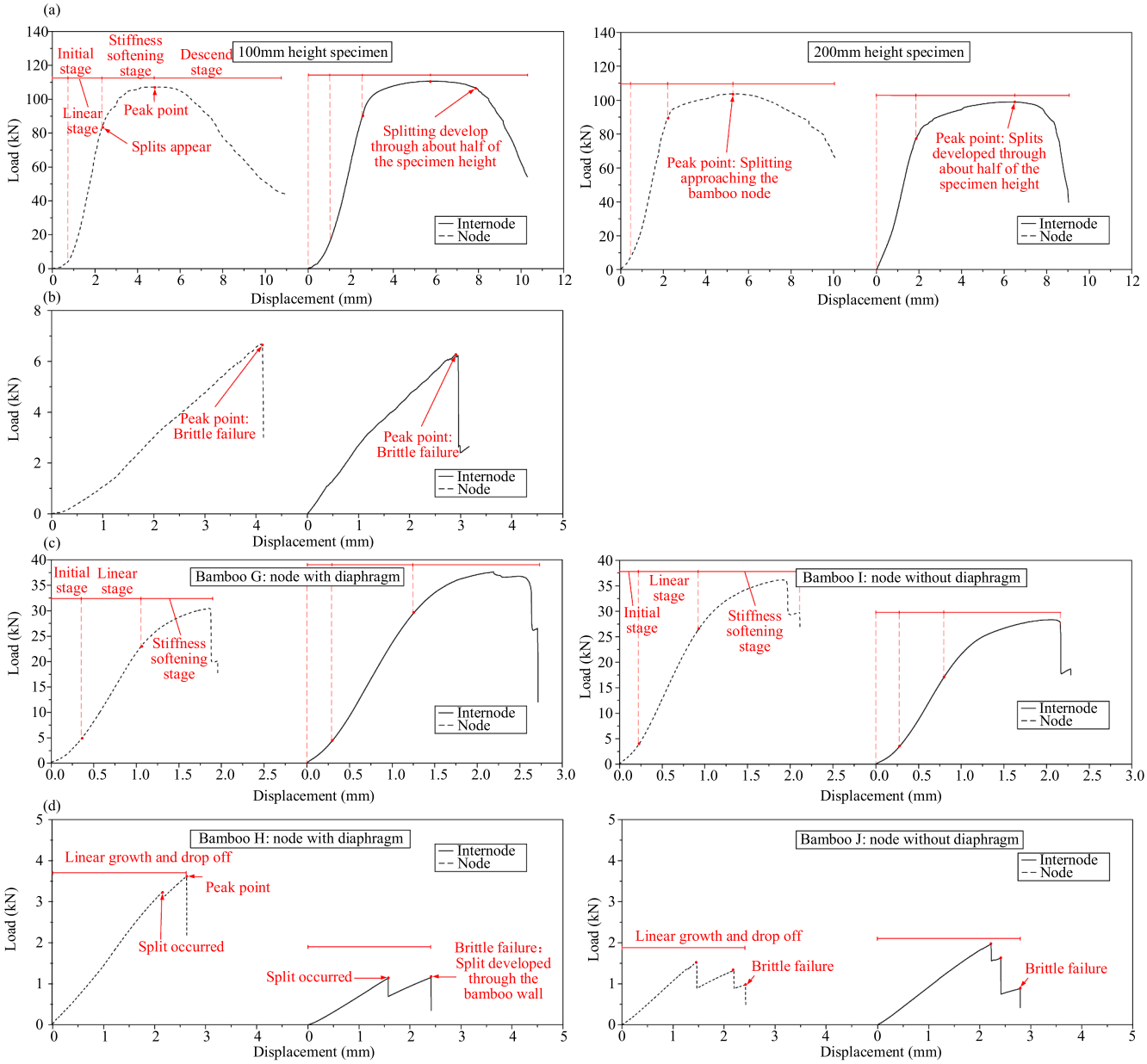

Fig. 8. Load-displacement curves of all specimens: (a) compressive specimens parallel to the grain, (b) tensile specimens parallel to the grain, (c) shear specimens parallel to the grain, and (d) radial compressive specimens.

height. In addition, the rule of discreteness of the compressive strength of specimens of 200 mm height was different from that of 100 mm specimens. For compressive node specimens with a height of 100 mm, the complex arrangement of bamboo fibers near the node [28] increased the unpredictability of the compressive strength. As a result, the discreteness of the compressive strength of the node specimens was higher than that of the internode specimens. The coefficient of variation of the compressive strength of the node specimens was 9.16%, and thus was higher than the value of 7.05% for the internode specimens. However, for the compressive specimens of 200 mm height, the discreteness

Table 3
Summary of test results.

Specimen group	Specimen detail	Location	Strength (MPa)		Increment
			Internode	Node	
Compressive test parallel to the grain	Bamboo A	T	42.45(0.87)	45.31(1.74)	6.73%
	(100 mm)	M	41.52(1.00)	40.02(0.07)	−3.60%
		B	42.23(0.45)	37.87(0.91)	−10.34%
	Bamboo B	T	47.71(1.93)	48.00(0.45)	0.60%
	(100 mm)	M	43.73(0.90)	43.08(1.77)	1.49%
		B	39.01(1.43)	39.49(0.66)	1.23%
	Bamboo C	T	43.97(0.94)	39.58(1.83)	−9.97%
	(200 mm)	M	41.16(0)	41.38(0.65)	0.53%
		B	38.58(2.97)	39.70(3.24)	2.90%
	Bamboo D	T	33.43(1.69)	35.30(1.27)	5.61%
	(200 mm)	M	32.91(0.01)	33.68(1.23)	2.36%
		B	30.07(2.39)	32.03(1.78)	6.51%
Tension test parallel to the grain	Bamboo E	T	162.59(0.90)	85.74(9.98)	−47.27%
		M	152.96(6.92)	83.29(5.22)	−45.54%
		B	174.30(3.60)	73.66(2.79)	−57.74%
	Bamboo F	T	138.57(10.38)	84.29(1.56)	−39.17%
		M	143.09(1.67)	74.99(0.73)	−47.59%
		B	134.83(7.80)	76.66(9.00)	−43.14%
Shear test parallel to the grain	Bamboo G	T	9.47(0.83)	10.41(0.54)	9.93%
		M	10.41(1.18)	11.30(0.40)	8.55%
		B	11.15(0.96)	11.03(0.80)	−1.08%
	Bamboo I	T	10.79(0.42)	10.71(0.98)	0.74%
	(without diaphragm)	M	11.90(0.90)	11.83(0.48)	10.46%
		B	11.37(0.43)	12.54(0.23)	10.29%
			Pipe stiffness (Pa)		
Radial compressive test	Bamboo H	T	7040.83(366.12)	15703.28(1471.39)	123.01%
		M	6675.39(637.86)	16350.45(1796.52)	144.94%
		B	7766.67(169.96)	15925.49(1460.09)	105.04%
	Bamboo J	T	9675.01(258.60)	10200.73(845.58)	3.36%
	(without diaphragm)	M	9700.05(234.52)	9825.21(369.97)	1.29%
		B	7933.33(286.74)	9225.38(521.41)	16.28%

Note: The values in brackets are the standard deviation of the strength.

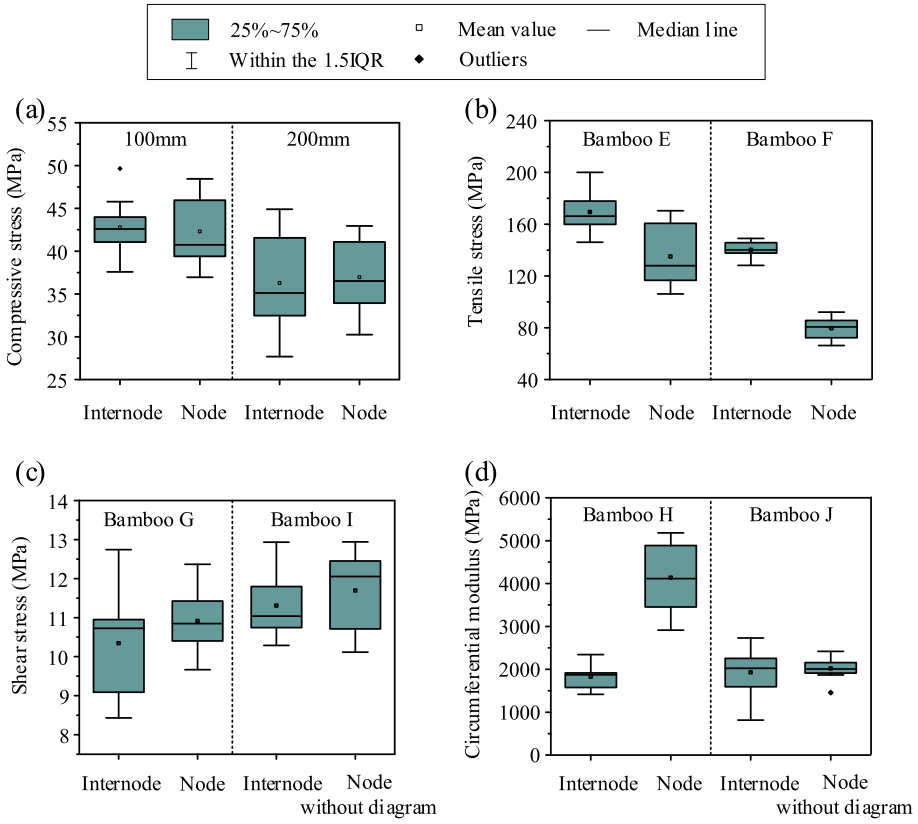

Fig. 9. Boxplots of strength or pipe stiffness of (a) compressive specimens parallel to the grain, (b) tensile test parallel to the grain, (c) shear test parallel to the grain, and (d) radial compressive specimens.

of the compressive strength of node specimens was lower than that of internode specimens. The coefficient of variation of the compressive strength of specimens was 11.09% (node) and 15.23% (internode). It is reasonable in consideration of the failure modes. The bamboo node of the 200 mm specimens was not broken when reaching the peak load. In this regard, the complex arrangement of bamboo fibers at the node had little influence on the load-carrying capacity. Besides, the bamboo node effectively functions as a rib in the middle of the 200 mm specimen, resulting in the specimen being less prone to buckling.

Fig. 9(b) shows the tensile strength of the node and internode specimens. The average tensile strength of the node specimens was significantly lower than that of the internode specimens. Meanwhile, the discreteness of the tensile strength of the node specimens was higher than that of the internode specimens. Similarly, the complex arrangement of bamboo fibers made the tensile strength of node specimens more unpredictable than that of internode specimens with longitudinally arranged fibers.

Fig. 9(c) shows the boxplots of shear strength. The average shear strength of the node specimens with or without the diaphragm was slightly higher than that of the internode specimens since the bamboo node restrained the relative slip of shear surfaces, as shown in Fig. 6. The discreteness of the shear strength of node specimens was lower than that of internode specimens in bamboo G. The coefficient of variation of the shear strength of node specimens in bamboo G was 6.79%, and thus was lower than 12.25% of internode specimens. However, the specimens in bamboo I showed the opposite result, and the coefficient of variation of the shear strength of the node specimens without a diaphragm in bamboo I was 8.50%, and hence was higher than the 6.52% of the internode specimens. It might be deduced that the diaphragm is the key issue in reducing the discreteness and improving the shear strength.

Fig. 9(d) shows the pipe stiffness of the radial compressive specimens. The average pipe stiffness of the node specimens with a diaphragm was approximately twice as high as that of the internode specimens, while the value of the node specimens without a diaphragm was almost the same as that of the internode specimens. The existence of the diaphragm changed the force transmission path when subjected to radial load, thus reducing the bending moment on the bamboo culm. Therefore, the diaphragm could improve the mechanical behavior of the specimen. Nonetheless, the node specimens with a diaphragm also showed larger discreteness of the pipe stiffness due to the irregular shape of the diaphragm.

4.2. Effect of the node and position of the specimen

Analysis of Variance (ANOVA) is a statistical method used to compare means between two or more groups. It determines whether the differences observed in sample means are statistically significant. In ANOVA, the null hypothesis assumes that there is no significant difference between the means of the groups being compared. The alternative hypothesis suggests that there is at least one group whose mean is significantly different from the others. In this section, ANOVA was performed to evaluate the effects of the node and height position on the characteristic values. The ANOVA was conducted using SPSS software, and the results are presented in Table 4.

The F is calculated by comparing the variability between the group means to the variability within the groups. The independent variable $F1$ indicated the existence of a node or internode, and $F2$ represented the height position of the specimen at the bottom, middle, or top of the culm. The interaction effect includes simultaneous effects of the two variables. The calculation of F is as follows:

$$SSW = \sum (x_i - \bar{x}_i)^2$$

$$SSB = \sum (\bar{x}_i - \bar{\bar{x}})^2$$

$$df_{\text{between}} = k - 1$$

$$df_{\text{within}} = N_T - k$$

$$F = \frac{SSB/df_{\text{between}}}{SSW/df_{\text{within}}}$$

where SSW represents the sum of squares within. $(x_i\text{-}\bar{x}_i)$ represents each data point minus its respective group mean. SSB represents the sum of squares between. $(\bar{x}_i\text{-}\bar{\bar{x}})$ represents the group means minus the overall mean of the entire dataset. df_{between} represents the degrees of freedom between groups. k represents the number of groups being compared. df_{within} represents the degrees of freedom within groups. N_T represents the total number of observations.

The P-value associated with the F is a measure of the strength of evidence against the null hypothesis. It indicates the probability of observing an F value as extreme as, or more extreme than, the one calculated from the data, assuming that the null hypothesis is true.

The F is used to compare the variability between groups (SSB) with the variability within groups (SSW). If the F is large and the corresponding P-value is less than a chosen significance level (take 0.05 in the analysis), it suggests that the variability between groups is significantly greater than the variability within groups.

The impact of nodes on compressive strength parallel to the grain was assessed for specimens of 100 mm and 200 mm in length. The results showed that the P-values of nodes for 100 mm and 200 mm specimens were 0.61 and 0.74, respectively, indicating a negligible influence on compressive strength. Regarding height position, 100 mm specimens had a significant effect on compressive strength with a P-value of 0.00. This implies a correlation between the height position and the compressive strength of bamboo. However, for 200 mm specimens, height position had a marginal impact on compressive strength with a significance value of 0.52. Due to the large slenderness ratio of the

Table 4
Influence of the node, internode, and height position on the mechanical properties.

Mechanical properties		Analysis of ANOVA					
		Main effect				Interaction effect	
		$F1$	P	$F2$	P	$F1$*$F2$	P
		(Existence of the node)		(Height position)			
Compressive strength	100 mm	0.26	0.61	14.96	0.00**	6.70	1.28
	200 mm	0.11	0.74	0.68	0.52	0.22	0.81
Tensile strength		14.40	0.00**	0.29	0.76	0.01	0.99
Shear strength	Diaphragm	2.15	0.16	3.22	0.06	0.78	0.47
	Without diaphragm	1.25	0.28	6.78	0.01*	1.97	0.17
Pipe stiffness	Diaphragm	232.97	0.00**	0.228	0.80	0.59	0.56
	Without diaphragm	6.23	0.02*	11.67	0.00**	2.28	0.13

Note: * means P-value in the calculation smaller than probability 5 % but greater than 1 % ($0.01 < P < 0.05$), ** means P-value in the calculation smaller than probability 1 % ($P < 0.01$).

specimen, force eccentricity may occur in compression experiments, which may cause the specimen to buckle before yielding. For the tensile strength parallel to the grain, the results showed that the node had a significant influence on the tensile strength with a *P*-value of 0.00. Combining the strength data in Table 3, it can be concluded that the tensile strength of bamboo was significantly weakened by bamboo nodes. The height position had a negligible influence with a *P*-value of 0.76. For shear strength parallel to the grain, the *P*-values of the node on shear strength in bamboo G (node with diaphragm) and bamboo I (node without diaphragm) were 0.16 and 0.28, respectively. In this regard, the bamboo node showed a negligible influence on the shear strength. The *P*-values of height position on shear strength in bamboo G and bamboo I were 0.06 and 0.01, respectively, indicating a significant effect on the shear strength.

For the radial compressive test, the *P*-values of the node on pipe stiffness in bamboo H (node with diaphragm) and bamboo J (node without diaphragm) were 0.00 and 0.02, respectively. That is, the bamboo node showed a significant influence on the pipe stiffness. By combining the pipe stiffness data in Table 3, it can be concluded that the pipe stiffness of bamboo was significantly strengthened by bamboo nodes. In addition, the *P*-values of height position on pipe stiffness in bamboo H and bamboo J were 0.80 and 0.00, respectively, indicating that the height position showed a significant effect for bamboo J (node without diaphragm) but a negligible influence for bamboo H (node with diaphragm). The irregular shape of the diaphragm from top to bottom led to different contributions to the radial capacity [29], interfering with the correlation of bamboo H specimens in the height position effect.

The *P*-values of the interaction of variances on four kinds of strength were all larger than 0.01, indicating a negligible influence on the strength.

4.3. Strain distribution

The load–strain curves of the radial compressive specimens to evaluate the effect of nodes are shown in Fig. 10. Fig. 10(a) shows the load–strain relationships for bamboo H. The strain of the node specimen was much lower than that of the internode specimen due to the existence of the diaphragm. In addition, the strain distribution was consistent with the structural analysis, but the values were different from the theoretical results based on the circular cross section due to the irregular shape of natural bamboo culms.

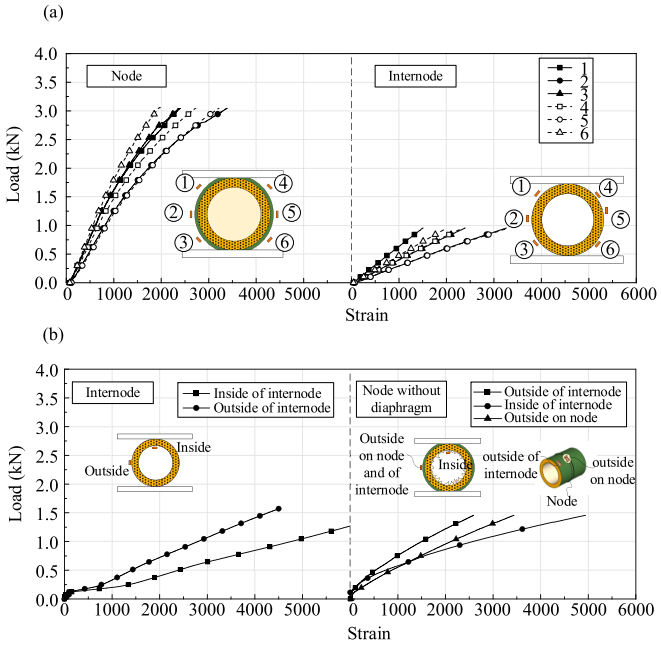

Fig. 10. Load-strain curves for (a) internode and node specimens in bamboo H, and (b) internode and node specimens in bamboo J.

Fig. 10(b) shows the load–strain curves for bamboo J in which the diaphragm was removed from the node specimen. The tensile strain inside the bamboo culm was higher than that outside the culm due to the concentrated load, but cracks first occurred at the outside surface at both ends of the major axis since the elastic modulus inside the bamboo culm was lower than that of the outside [19]. It was also found that the strain on the outside surface at the node region was less than that of the corresponding internode part for the node specimens. Even if the diaphragm had been removed, the remaining portion of the node exhibited a higher stiffness than the bamboo culm.

5. Discussion based on fiber morphology

5.1. Effect of the node

In previous studies, the morphology and volume fraction of bamboo fibers have been investigated to analyze the specific mechanical properties of the node and internode specimens [30–33]. In this section, a comprehensive discussion based on fiber morphology is presented to explain the effect of nodes under different load conditions.

The longitudinal section view of the bamboo node is shown in Fig. 11 (a). When the longitudinal fibers at the internode passed through the bamboo node, the fibers swelled, and some deflected into the diaphragm [16,34]. In addition, the fibers twist at the joint between the diaphragm and bamboo culm [35,36]. Fig. 11(b) shows the transverse section view of the diaphragm under light exposure. The fibers in the diaphragm were randomly arranged and interlaced. In this regard, the diaphragm could be seen as transverse isotropy.

Fig. 11 shows the observations of fiber arrangement and morphology at the node from different perspectives. Based on the observations in Fig. 11, a schematic of specimens under mechanical tests parallel to the grain is proposed in Fig. 12. The purpose of Fig. 12 is to explain the effect of nodes under different load conditions.

For the compressive tests parallel to the grain, the fibers of the internode specimens buckled, as shown in Fig. 12(a). However, for the node specimens, buckling occurred away from the bamboo node due to the restraint from the fibers of the diaphragm. Fig. 12(b) shows the mechanism of tensile specimens parallel to the grain. The internode specimen fractured after the fiber reached its tensile strength. For the node specimen, some longitudinal fibers twisted or deflected into the diaphragm, decreasing the number of fibers subjected to the tensile load. As a result, the bamboo node became defective compared to the internode. In addition, the fracture would first appear at the inner side of the bamboo culm, where the fiber deflected into the diaphragm. Fig. 12(c) shows the mechanical behaviors based on fiber morphology in shear tests. For internode specimens, parenchyma tissue was separated from fiber along the shear surface. As the relative slip of the shear surface develops, the parenchyma tissue collapses [28]. For the node specimens, the shear strength provided by parenchyma tissue at the bamboo node was lower than that of the internode due to the lower fraction of parenchyma tissue at the node [18]. Nonetheless, the twisted fibers and diaphragm both contributed to the shear resistance. Consequently, the bamboo node showed a negligible influence on the shear strength considering the negative effect of the lower fraction of parenchyma tissue and the positive effect of twisted fibers and the diaphragm.

5.2. Effect of the diaphragm

In the radial compressive test, the diaphragm could prevent splitting at both ends of the major axis. In this section, a compressive test of the diaphragm was conducted, and then the mechanism of the bamboo diaphragm under radial compression was analyzed. Due to the small size and the large undulations of the diaphragm, it was difficult to obtain large and flat coupons. Therefore, coupons were only obtained with

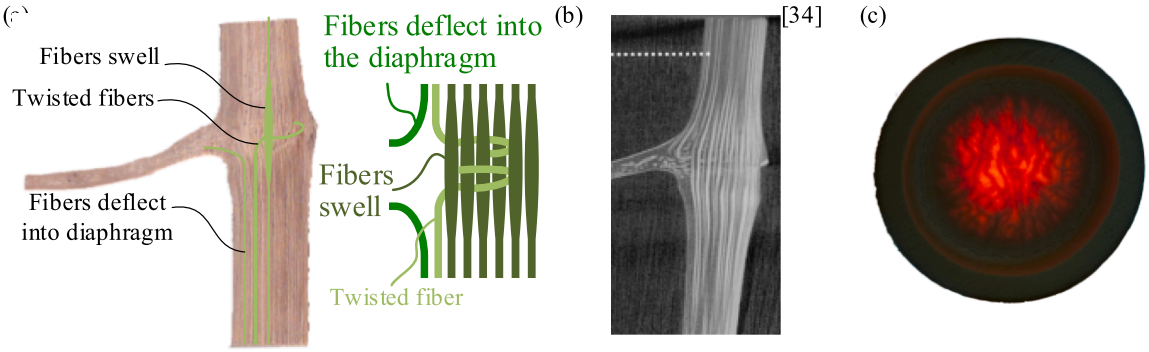

Fig. 11. Fiber arrangement based on the node morphology. (a) Longitudinal section view, (b) CT-scanned longitudinal section view [36], and (c) transverse section view of the diaphragm under light exposure.

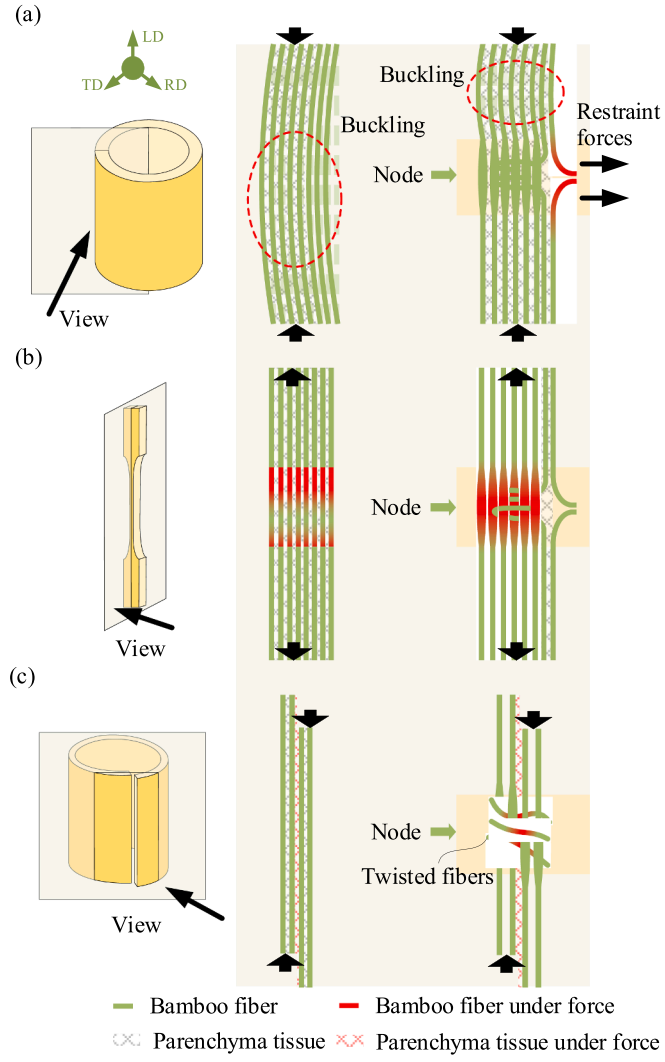

Fig. 12. Schematic of the bamboo node and internode specimens under mechanical tests parallel to the grain: (a) compressive test, (b) tensile test, (c) shear test.

small sizes in the center of the diaphragm. However, from another perspective, the small size coupon could also avoid instability during compression. The test referred to the standard for composite material GB/T 1448–2005 [37]. Eight coupons with a width of 10 mm and a height of 5.2 mm were taken from four adjacent nodes in the middle of a bamboo culm, and this was among the culms for the above mechanical tests. The thickness of the diaphragm was approximately 1.8 mm. The coupons and experimental setup are shown in Fig. 13(a). The stress-displacement curves and the failure mode are shown in Fig. 13(b). The average compressive strength of the coupons is 31.32 MPa, indicating that the diaphragm has a certain strength that can contribute to the mechanical properties of bamboo nodes. The coupons were cut from different directions in the diaphragm, but the coefficient of variation of the test results was only 6.29%, confirming the assumption of transverse isotropy of the diaphragm raised by the fiber morphology.

A schematic view of the radial compressive specimen is shown in Fig. 14. Fig. 14(a) shows the mechanical behavior of the internode specimen. The bending moment on the ends of the major and minor axes was larger than the rest of the culm. As a result, splitting occured at or near the end of the axis. Fig. 14(b) shows the failure modes of the node specimens. When loaded at both ends of the minor axis, uniformly distributed tensile stress was generated within the core of the diaphragm. Therefore, the failure mode was characterized by fracture of the diaphragm. In addition, the diaphragm provided support against compression, significantly improving the radial compressive strength.

6. Conclusion

In this work, the effects of bamboo nodes on the mechanical properties of bamboo culms were tested and analyzed. A total of 168 specimens divided into four types were tested, including compressive, tensile, shear tests parallel to the grain and radial compressive tests. The load–displacement curves and failure modes were analyzed. The analysis of variance method was used, and a comprehensive discussion based on fiber morphology is presented to explain the effect of nodes under different load conditions. The following conclusions can be drawn:

1. The presence of bamboo nodes in the culm resulted in a reduction of tensile strength by 47% but resulted in a reinforcement of pipe stiffness by 123%. However, no significant effect was observed in compressive and shear strength. In the case of compressive specimens with varying heights, nodes only exhibited local effectiveness, except for buckling.
2. The results of the analysis of variance indicated that the compressive strength of 100 mm specimens, shear strength and pipe stiffness of node specimens without a diaphragm showed changes along different sampling heights. However, no evidence showed that the enhanced effects of the bamboo node were related to the sampling height.
3. The node and internode specimens show different mechanical properties and behaviors due to the different morphology and volume fraction of fiber between the node and internode. In compressive tests parallel to the grain, the deflected fiber constrained the buckling near the node of the natural bamboo. In tensile tests parallel to the grain, the tensile strength of node specimens decreases since

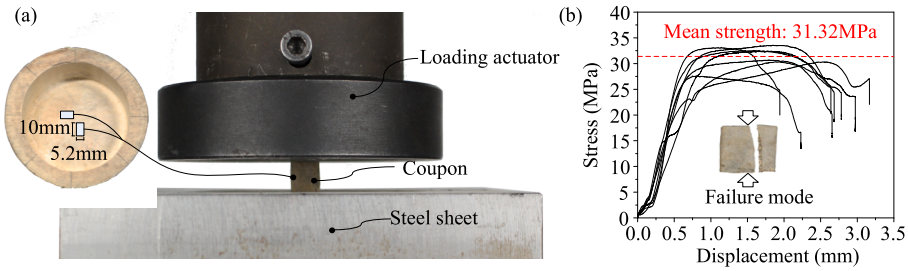

Fig. 13. Test setup and results of the bamboo diaphragm: (a) Coupon process and test setup, and (b) stress-displacement curve of the bamboo diaphragm.

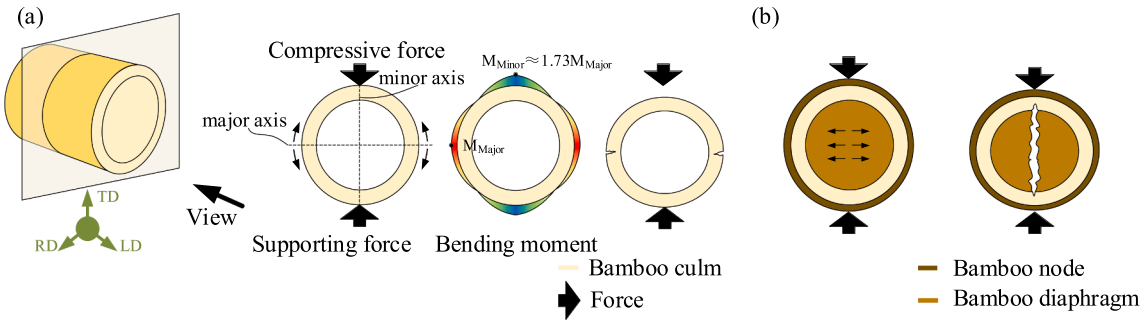

Fig. 14. Mechanical behaviors and effect of the diaphragm in the radial compressive test. (a) Mechanical behavior of the internode specimen, and (b) failure modes of the node specimens.

some fibers twist repeatedly at the bamboo node or deflect into the bamboo diaphragm, decreasing the total amount of bamboo fibers subjected to the tensile load. In shear tests parallel to the grain, twisted fibers increase the shear strength, but the lower fraction of parenchyma tissue decreases the shear strength of the node. The bamboo node showed a negligible influence on the shear strength.

4. The diaphragm can be considered an isotropic material. The compressive strength of the bamboo diaphragm was 31.32 MPa. In radial compressive tests, the load bearing capacity of node specimens is significantly strengthened due to the existence of the bamboo diaphragm.

CRediT authorship contribution statement

Xinmiao Meng: Conceptualization, Methodology, Supervision, Writing – original draft, Project administration, Funding acquisition. **Zhancheng Zhang:** Investigation, Data curation, Validation, Writing – review & editing. **Youde Wu:** Investigation, Data curation, Writing – review & editing. **Feiyang Xu:** Investigation, Formal analysis. **Peng Feng:** Conceptualization, Supervision, Project administration, Writing – review & editing.

Declaration of Competing Interest

The authors declare that they have no known competing financial interests or personal relationships that could have appeared to influence the work reported in this paper.

Data availability

No data was used for the research described in the article.

Acknowledgments

The authors acknowledge the funding supported by the National Natural Science Foundation of China (No. 51908038).

References

[1] Xu X, Xu P, Zhu J, et al. Bamboo construction materials: Carbon storage and potential to reduce associated CO_2 emissions. Sci. Total Environ. 2015;814:152697. https://doi.org/10.1016/j.scitotenv.2021.152697.
[2] Yan L, Zhang Z, Zhang Y, et al. Evaluation of the effect of thickness moisture content of laminated bamboo strips on thermoforming temperature. In: 18th International Conference on Non-conventional Materials and Technologies (NOCMAT 2022); 2022. https://doi.org/10.5281/zenodo.6599495.
[3] Nie S, Ran S, Wu D, et al. Mechanical properties of Moso bamboo connections with external clamp steel plates. J. Renewable Mater. 2022;10(2):487–510. https://doi.org/10.32604/jrm.2022.017275.
[4] Xiang E, Yang S, Cao C, et al. Visualizing complex anatomical structure in bamboo nodes based on X-ray microtomography. J. Renewable Mater. 2021;9(9):1531–40. https://doi.org/10.32604/jrm.2021.015346.
[5] Taylor D, Kinane B, Sweeney C, et al. The biomechanics of bamboo: investigating the role of the nodes. Wood Sci. Technol. 2015;49:345–57. https://doi.org/10.1007/s00226-014-0694-4.
[6] Shao Z, Zhou L, Liu Y, et al. Differences in structure and strength between internode and node sections of Moso bamboo. J. Trop. For. Sci. 2010;22(2):133–8.
[7] Li S, Yang S, Shang L, et al. 3D visualization of bamboo node's vascular bundle. Forests 2021;12(12):1799. https://doi.org/10.3390/f12121799.
[8] Liu S, Tong Z, Tang Z, et al. Bionic design modification of non-convex multi-corner thin-walled columns for improving energy absorption through adding bulkheads. Thin-Walled Struct. 2015;88:70–81. https://doi.org/10.1016/j.tws.2014.11.006.
[9] Zou M, Xu S, Wei C, et al. A bionic method for the crashworthiness design of thin-walled structures inspired by bamboo. Thin-Walled Struct. 2016;101:222–30. https://doi.org/10.1016/j.tws.2015.12.023.
[10] Yusuf A, Harries KA, Flower CV, et al. Through-culm wall mechanical behaviour of bamboo. Constr. Build. Mater. 2019;216:485–95. https://doi.org/10.1016/j.conbuildmat.2019.04.214.
[11] Zhong Z, Zhou X, He Z, et al. Creep behavior of full-culm Moso bamboo under long-term bending. Journal of Building Engineering 2022;46:103710. https://doi.org/10.1016/j.jobe.2021.103710.
[12] Themelina P, Pradhan NPN, Stoura CD, et al. Monotonic loading testing and characterization of new multi-full-culm bamboo to steel connections. Constr. Build. Mater. 2019;201(20):473–83. https://doi.org/10.1016/j.conbuildmat.2018.12.198.
[13] Liu P, Zhou Q, Fu F, et al. Effect of bamboo nodes on the mechanical properties of P. edulis (Phyllostachys edulis) bamboo. Forests 2021;12(10). https://doi.org/10.3390/f12101309.
[14] Nie S, Fu W, Wang H, et al. Experimental study of Moso bamboo to-steel connections with embedded grouting materials. J. Renew. Mater. 2023;11(3):023446. https://doi.org/10.32604/jrm.2022.023446.
[15] Oka G, Triwiyono A, Awaludin A, et al. Effects of node, internode and height position on the mechanical properties of Guanochlor Atroviolacea bamboo. Procedia Eng. 2014;95:31–7. https://doi.org/10.1016/j.proeng.2014.12.162.
[16] Huang X, Li F, Hoop C, et al. Analysis of Bambusa rigida bamboo culms between internodes and nodes: anatomical characteristics and physical-mechanical

properties. For. Prod. J. 2018;68(2):157–62. https://doi.org/10.13073/FPJ-D-17-00035.
[17] Srivaro S, Jacanid W. Comparison of physical and mechanical properties of Dendrocalamus asper Backer specimens with and without nodes. Eur. J. Wood Wood Prod. 2016;74(6):893–9. https://doi.org/10.1007/s00107-016-1048-8.
[18] Chen G, Luo H. Effects of node with discontinuous hierarchical fibers on the tensile fracture behaviors of natural bamboo. Sustain. Mater. Technol. 2020;26. https://doi.org/10.1016/j.susmat.2020.e00228.
[19] Sharma B, Harries KA, Ghavami K. Methods of determining transverse mechanical properties of full-culm bamboo. Constr. Build. Mater. 2013;38:627–37. https://doi.org/10.1016/j.conbuildmat.2012.07.116.
[20] Moran R, Webb K, Harries K, et al. Edge bearing tests to assess the influence of radial gradation on the transverse behavior of bamboo. Constr. Build. Mater. 2017;131:574–84. https://doi.org/10.1016/j.conbuildmat.2016.11.106.
[21] Lee PH, Odlin M, Yin H, et al. Development of a hollow cylinder test for the elastic modulus distribution and the ultimate strength of bamboo. Constr. Build. Mater. 2014;51:235–43. https://doi.org/10.1016/j.conbuildmat.2013.10.051.
[22] García J, Rangel C, Ghavami K, et al. Experiments with rings to determine the anisotropic elastic constants of bamboo. Constr. Build. Mater. 2012;31:52–7. https://doi.org/10.1016/j.conbuildmat.2011.12.089.
[23] Pradhan N., Mouka T., Lee Y., et al. Edge bearing induced failure of full culm bamboo, Global Bamboo and Rattan Congress 2018 (BARC 2018), Beijing, China. 2018; 25-27.
[24] ISO 22157-2019, Bamboo structures — Determination of physical and mechanical properties of bamboo culms — Test methods, The International Standardization Organization, 2019.
[25] JGT 199-2007, Testing methods for physical and mechanical properties of bamboo used in building, Ministry of Housing and Urban-Rural Development of the People's Republic of China, Beijing, 2007. (in Chinese).
[26] GB/T 9647-2015, Thermoplastics pipes — Determination of ring stiffness, China Standards Press, Beijing, 2015. (in Chinese).
[27] ASTM D2412-96a, Standard test method for determination of external loading characteristics of plastic pipe by parallel-plate loading, ASTM International, West Conshohocken, 2002.
[28] Huang A, Su Q, Zong Y, et al. Study on different shear performance of Moso bamboo in four test methods. Polymers 2022;14(13):2649. https://doi.org/10.3390/polym14132649.
[29] Meng X, Sun H, Cao Y, et al. Experimental study on uniaxial compression of bamboo nodes using 3D scanning technique. MATEC Web of Conferences 2019;275(10):01022. https://doi.org/10.1051/MATECCONF/201927501022.
[30] Okubo K, Fujii T, Yamamoto Y, et al. Development of bamboo-based polymer composites and their mechanical properties. Compos. A 2003;35(3):377–83. https://doi.org/10.1016/j.compositesa.2003.09.017.
[31] Khalil H, Bhat I, Jawaid M, et al. Bamboo fiber reinforced biocomposites: A review. Mater. Des. 2012;42:353–68. https://doi.org/10.1016/j.matdes.2012.06.015.
[32] Trujillo E, Moesen M, Osorio L, et al. Bamboo fibers for reinforcement in composite materials: Strength Weibull analysis. Compos. A 2014;61:115–25. https://doi.org/10.1016/j.compositesa.2014.02.003.
[33] Shang L, Sun Z, Liu X, et al. A novel method for measuring mechanical properties of vascular bundles in mosso bamboo. J. Wood Sci. 2015;61(6):562–8. https://doi.org/10.1007/s10086-015-1510-y.
[34] Liese W, Tang TKH. Properties of the bamboo culm. Switzerland: Springer International Publishing; 2015. p. 227–56.
[35] Peng G, Jiang Z, Liu X, et al. Detection of complex vascular system in bamboo node by X-ray μCT imaging technique. Holzforschung 2014;68(2):223–7.
[36] Huang P, Chang WS, Ansell MP, et al. Density distribution profile for internodes and nodes of Phyllostachys edulis (Moso bamboo) by computer tomography scanning. Constr. Build. Mater. 2015;93:197–204. https://doi.org/10.1016/j.conbuildmat.2015.05.120.
[37] GB/T 1448-2005, Fiber-reinforced plastics composites — Determination of compressive properties, China Standards Press, Beijing, 2005. (in Chinese).